American Mineralogist, Volume 92, pages 1018–1025, 2007

The high-pressure crystal structure of potassium hydrogen carbonate ($KHCO_3$)

D.R. Allan,[1,*] W.G. Marshall,[2] and C.R. Pulham[1]

[1]School of Chemistry and Centre for Science at Extreme Conditions, The University of Edinburgh, West Mains Road, Edinburgh, EH9 3JJ, U.K.
[2]ISIS Facility, CCLRC Rutherford Appleton Laboratory, Chilton, Didcot, OX11 0QX, U.K.

Abstract

The crystal structure of the high-pressure phase of potassium hydrogen carbonate, here termed $KHCO_3$ form III, has been solved using single-crystal X-ray diffraction techniques. It adopts triclinic $P\bar{1}$ symmetry and is formed on direct compression of the monoclinic ambient-pressure phase (kalicinite, form I) via a first-order phase transition at 3.2 GPa ($\Delta V/V$ ~4%). We have also used time-of-flight high-pressure neutron powder-diffraction to determine the structural changes in $KDCO_3$ of the form I and III polymorphs to 8.3 GPa. This study indicates that the transition appears to be in response to pronounced displacements of the K^+ cations and the cooperative tilting of the $(DCO_3^-)_2$ dimers. The O···O hydrogen bond distance shows a monotonic compression over the entire pressure range studied with no obvious discontinuity at the phase transition. However, the O-D···O bond angle appears to exhibit an abrupt ~4° decrease across the I–III phase transition with a concomitant change in its pressure dependence. Birch Murnaghan fits to the equation of state data above and below the transition indicate that form III [B_0 = 26.5(2.8) GPa, B' = 5.2(6)] is marginally less compressible than form I [B_0 = 22.7(8) GPa, B' = 4.1(5)].

Keywords: Kalicinite, high-pressure, crystal structure, phase transition

Introduction

The behavior of hydrous mineral phases under conditions of high pressure is of fundamental importance to geological processes occurring in the Earth's interior. For example, dehydration reactions in subducting slabs are often associated with volcanic activity at the Earth's surface and with the triggering of deep-focused earthquakes. Many of the hydrous minerals in subduction zones act as water "sinks," often containing several wt% of water, and so are of crucial importance to the water budget of the mantle. Minerals such as carbonates and bicarbonates (or hydrogen carbonates) act as sinks for carbon dioxide, and there is increasing interest in these materials as a means of combating global warming by sequestration of the CO_2 produced by the combustion of fossil fuels. Hydrogen bonding plays a pivotal role in the relative structural stability of these minerals and as a consequence a range of high-pressure spectroscopic and diffraction techniques have been used to examine the effect of compression on the hydrogen bond. Among these minerals kalicinite (potassium bicarbonate, $KHCO_3$) has attracted significant recent attention, not only on account of its relatively simple structure, but also because of the unusually strong hydrogen bonding observed in the structure at ambient pressure. This system is also of more fundamental interest on account of the diffuse scattering observed from single crystals of $KHCO_3$ at low temperature that has been interpreted in terms of long-range quantum wavefunction entanglement of the indistinguishable protons (Fillaux et al. 2003; Keen and Lovesey 2003; Fillaux and Cousson 2004).

Under ambient conditions $KHCO_3$ crystallizes from aqueous solution in the monoclinic $P2_1/a$ space group (form I—kalicinite) (Nitta et al. 1952; Thomas et al. 1974). The structure is characterized by the presence of strongly hydrogen bonded $(HCO_3^-)_2$ dimers which are disposed on planes parallel to $(\bar{3}01)$. The potassium cations are coordinated to eight oxygen atoms from six HCO_3^- anions, and it is this coordination environment which bridges the otherwise isolated dimers. With a relatively short O···O separation of 2.656(4) Å, an H···O distance of 1.64(1) Å and an O-D···O angle of 175.9(6)° (Kagi et al. 2003), the hydrogen bonding within the structure is relatively strong. The hydrogen atoms are all crystallographically equivalent and so their local dynamics can be represented with symmetric pairs of coupled oscillators. At temperatures below ~14 K, in the degenerate ground state, Pauli exclusion imposes proton spin correlation on the hydrogen atoms, which in turn separates their dynamics from those of the other atoms in the structure, resulting in long-range quantum entanglement. This effect has been probed by single-crystal neutron diffraction techniques in $KHCO_3$ and the resulting diffraction pattern exhibits rods of intensity, superimposed on the $P2_1/a$ structure reciprocal lattice. These features were attributed to a sublattice of protons acting as a regular array of double slits parallel to the dimer planes (Keen and Lovesey 2003), although the full theoretical interpretation of these results has been the subject of some debate (Fillaux and Cousson 2004).

* Present address: Diamond Light Source Ltd., Diamond House, Chilton, Didcot, Oxfordshire, OX11 0DE, U.K. E-mail: David.Allan@diamond.ac.uk

0003-004X/07/0007–1018$05.00/DOI: 10.2138/am.2007.2336

At 318 K, kalicinite undergoes a structural phase transition to the high-temperature form II (monoclinic, *C*2/*m*) (Kashida and Yamamoto 1990; Takasaka et al. 1997). This transformation involves a subtle orientational reordering of the dimers with an accompanying increase in symmetry. The hydrogen atoms are now fully disordered, at least at the non-local level, between the two symmetric minima of the potential formed along the hydrogen bond. More recently, Takasaka et al. (2002) have reported evidence of an apparent structural change, which is produced, on the application of shear stress to the sample. Based on their Brillouin scattering studies, they assigned the configuration of the dimers to be ferrodistortive in character on the application of shear, though they had no direct structural evidence for this designation. In comparison, the arrangement of the dimers in forms I and II are antiferrodistortive and disordered respectively (Takasaka et al. 2002).

Recent high-pressure studies at ambient temperature, using X-ray and neutron powder-diffraction and infrared and Raman spectroscopy, have shown that kalicinite undergoes a structural phase transition at approximately 2.8 GPa (Nagai et al. 2002; Kagi et al. 2003, 2005). Although these studies were able to track the structural changes on compression over the pressure range approaching the transition, the crystal structure of the high-pressure phase, here termed form III, was not determined or even indexed. More recently, Komatsu et al. (2005) have reported a high-pressure single-crystal study of kalicinite at 4.6 GPa where the observed reflections could be divided into two subsets that could be indexed on monoclinic and triclinic unit cells. Only the set of reflections assigned to the monoclinic phase were used for subsequent structure solution while the remaining group of reflections was used for indexing the triclinic cell—though no crystallographic details have yet been published of either phase. Here we report the crystal structure solution of the high-pressure phase (form III) of kalicinite formed on direct compression of form I, which we have solved using single-crystal X-ray diffraction techniques and confirmed with neutron powder diffraction. The high-pressure polymorph adopts triclinic $P\bar{1}$ symmetry and, in common with both of the ambient-pressure phases, is characterized by the presence of $(HCO_3^-)_2$ dimers which are formed across an inversion center. The persistence of the dimer motif contradicts the proposed structure of form III shown in Kagi et al. (2005). The dimers, which have fully ordered hydrogen bonds, are arranged on planes parallel to $(\bar{4}12)$. The principal mechanism of the structural phase transition appears to be an antiparallel displacement of neighboring molecular layers, with an accompanying alteration of the coordination environment of the potassium cations. In the $P2_1/a$ form I structure, the K^+ ions are coordinated to eight oxygen atoms, K–O < 3.2 Å from six HCO_3^- anions. For the $P\bar{1}$ form III structure, however, the K^+ coordination environment includes ten oxygen contacts from a total of seven HCO_3^- anions, including two O···O oxygen contacts from a single $(HCO_3^-)_2$ dimer.

Experimental methods

Crystal growth

Single crystals of $KHCO_3$ were obtained by slow recrystallization from aqueous solution of a sample (99% purity) obtained from May and Baker Laboratory Chemicals (Prolabo). One small block-shaped crystal was selected from the batch and loaded into the diamond-anvil cell. The powder sample of $KDCO_3$ for the neutron diffraction experiment was prepared by dissolution of $KHCO_3$ (3.0 g) in 20 cm^3 D_2O (Aldrich, 99.9 at% D), followed by evaporation under vacuum at ambient temperature. This process was repeated twice more to obtain the necessary degree of deuterium exchange.

High-pressure single-crystal diffraction

The high-pressure X-ray experiments were carried out using a Merrill-Bassett diamond anvil cell (40° half-opening angle), equipped with 600 μm culets and a tungsten gasket (Merrill and Bassett 1974). A 4:1 mixture of methanol/ethanol was used as a hydrostatic pressure medium. Although $KHCO_3$ is only slightly soluble in methanol or ethanol, the pressure medium was prepared as a saturated solution to minimize the possibility of the sample partially dissolving. A small ruby chip was also loaded into the cell as the pressure calibrant, with the ruby fluorescence method being utilized to measure the pressure (Forman et al. 1972). Measurements of the latter were carried out by excitation with the 632.417 nm line from a He-Ne laser, the fluorescence being detected with a Jobin-Yvon LabRam 300 Raman spectrometer. The pressure was increased to 5.5 GPa to place the sample safely within the stability regime of form III.

Single-crystal diffraction data were collected on a Bruker SMART APEX diffractometer equipped with graphite monochromated Mo*K*α radiation (λ = 0.71073 Å). Data were collected using ω-scans at eight settings of 2θ and φ; full details of data collection and processing procedures were as described by Dawson et al. (2004). A preliminary examination of the diffraction pattern, using the RLATT routine in the Bruker AXS software package, indicated that almost all the reflections could be indexed on a triclinic cell. The diffracted intensities were sharp and there was no evidence that the transition had caused any pulverization of the sample. Subsequent indexing and integration using the program SAINT (Bruker-AXS 2003), yielded unit-cell dimensions of a = 4.2133(2) Å, b = 5.2974(3) Å, c = 6.1443(9) Å, α = 108.934(10)°, β = 100.743(10)°, γ = 95.109(6)° based on 301 reflections covering 8.857° < 2θ < 48.355°. The unit-cell axes were subsequently commuted so that a more direct comparison could be made with the ambient-pressure monoclinic structure (see Table 1). The integrated intensity data were corrected for absorption with the programs SADABS (Sheldrick 2004) and SHADE (Parsons 2004). The structure of the new phase was solved by direct methods using the program SIR92

Table 1. Crystallographic data from the high-pressure single-crystal X-ray diffraction study of the triclinic, $P\bar{1}$, form III of potassium hydrogen carbonate, ($KHCO_3$), at 5.5 GPa

Crystal data	Data collection
$KHCO_3$	Bruker SMART diffractometer
M_r = 200.23	Mo*K*α radiation
Triclinic, $P\bar{1}$	ω-scans
a = 6.1443(9) Å	P = 5.5 GPa
b = 5.2974(3) Å	T = 293 K
c = 4.2133(2) Å	Absorption correction: multi scan
α = 95.109(6)°	(SADABS; Sheldrick, 2004)
β = 100.743(10)°	162 measured reflections
γ = 108.934(10)°	162 independent reflections
V = 125.78(2) Å^3	148 reflections with $I > 2.00\sigma(I)$
Z = 2	θ_{max} = 26.059°
D_x = 2.643 Mg m^{-3}	$h = -4 \rightarrow 4$
	$k = -6 \rightarrow 5$
	$l = -5 \rightarrow 4$
Refinement	
Refinement on F	$W = [1 - (F_o - F_c)^2/6.24\sigma^2(F)]^2/$
R = 0.0402	$[3.82T_o(x) + 5.71T_1(x) + 1.66T_2(x)]$
wR = 0.0461	where T_i are Chebychev polynomials
S = 1.1032	and $x = F_c/F_{max}$
	(Prince 1982; Watkin 1994)
$(\Delta/\sigma)_{max}$ = 0.000384	
$\Delta\rho_{max}$ = 0.30 e Å^{-3}	
$\Delta\rho_{min}$ = –0.27 e Å^{-3}	

	Fractional coordinates			Hydrogen bonding	
	x	*y*	*z*		
K1	0.2992(4)	0.1343(2)	0.29058(15)	O1-H1	1.023 Å
C1	0.2300(18)	0.5737(11)	0.9057(8)	H1···O2	1.516(7) Å
H1	0.0659	0.6921	0.5524	O2···O3	2.498(8) Å
O1	0.2073(12)	0.7774(7)	0.7471(6)	O1-H1···O2	159.0(3)°
O2	0.1054(14)	0.3326(8)	0.7682(6)		
O3	0.3693(14)	0.6405(8)	1.1718(7)		

(Altomare et al. 1994) and refined against $|F|$ using CRYSTALS, (Betteridge et al. 2003). Due to the low completeness of this initial data set, a second set of data was collected with the Merrill-Bassett cell mounted on the goniometer head in an alternative orientation (i.e., rotated by 120° around the diamond-anvil cell's threefold axis of symmetry). The atoms were refined against the merged data sets with isotropic displacement parameters and the data were of sufficient quality to allow the straightforward location of the hydrogen from a Fourier difference map. The hydrogen atom position was included in the refinement using a riding constraint and with U_{iso}(H) set to 1.2 U_{iso}(O) of its parent oxygen atom. Listings of crystal and refinement data are given in Table 1.

Although the phase transition involves a decrease in symmetry from monoclinic to triclinic, we observed no additional reflections in the diffraction pattern that were consistent with any likely twin domains. However, in light of the abstract published by Komatsu et al. (2005), we used RLATT to select reflections that could not already be attributed to the triclinic reciprocal lattice of form III. A subset of these weak reflections could be indexed on a monoclinic cell (albeit with a deviation of ~0.2° from the ideal 90° for one of the cell angles) with approximately twice the volume of that of form III. The data were insufficient to yield anything more than this rather poorly determined cell and we are hesitant to draw any firm conclusions regarding the origin of these reflections. Furthermore, we are unaware of any reported examples where a single crystal transforms to two distinctly different structural phases under hydrostatic conditions. It is plausible, however, that as $KHCO_3$ is weakly soluble in the methanol/ethanol pressure transmitting medium another phase has precipitated from solution on compression at a pressure close to the I → III transition.

High-pressure neutron powder diffraction

High-pressure neutron powder diffraction data were collected using the PEARL/HiPr diffractometer (ISIS 1996, 1997) at the ISIS spallation neutron source, located at the CCLRC Rutherford Appleton Laboratory, U.K. A lightly ground powder sample of $KDCO_3$ and a small ~1 mm diameter pellet of Pb (a suitable pressure marker) was loaded into a TiZr capsule gasket (Marshall and Francis 2002) and moistened with perdeuterated 4:1 methanol/ethanol pressure transmitting medium. The resulting capsule assembly was then compressed within a type V3b Paris-Edinburgh (P-E) press (Nelmes et al. 1994; Besson et al. 1992) equipped with standard single toroid anvils with cemented WC cores (Ni binder). The ram pressure was monitored and controlled by means of a computer-controlled hydraulic system.

Time-of-flight (TOF) neutron powder diffraction data suitable for structure refinement were obtained by electronically forming the 1080 individual detector element spectra from the main PEARL/HiPr $2\theta = 90°$ detector bank. The resulting summed pattern was then normalized with respect to the incident beam monitor and the scattering from a vanadium calibration sample. Lastly, the diffraction pattern intensity scale was corrected for the wavelength and scattering-angle dependence of the neutron attenuation by the anvil (WC) and gasket (TiZr) materials. Full-profile Rietveld refinements of the TOF neutron powder diffraction patterns were carried out using the GSAS package (Larson and Von Dreele 2000). Sample pressures were calculated from the refined Pb lattice parameters and the room-temperature equation of state of lead as derived by Fortes (2004) from an average of the values in Kuznetsov et al. (2002), Miller and Schuele (1969) and Waldorf and Alers (1962).

All of the neutron diffraction patterns were collected on pressure increase, with P-E press loads ranging from the initial gasket sealing load of 7 tonnes up the maximum of 74 tonnes, the aim being to determine the pressure dependence of the structures of forms I and III and to locate the I–III phase transition pressure. Data collection times ranged between 3 and 7 h at an equivalent of 175 μA ISIS proton current. The sequence of powder-patterns obtained from the experiment is shown in Figure 1. The onset of the phase transition is observed at 3.16(5) GPa and it is complete by 3.45(5) GPa. The structural refinements were conducted with the GSAS suite of programs without the use of either restraints or constraints (Larson and Von Dreele 2000). Details of the individual data collections are given in Tables 2a and 2b along with the corresponding pressures, as determined from the Pb equation of state.

Figure 2b shows the final Rietveld refinement of the 41 tonnes load pattern (corresponding to a pressure of 3.45 GPa), which used the X-ray structure as the starting model. The first stage of this process involved finding suitable estimates for the lattice parameters, as the pressure here was some ~2.1 GPa less than in the X-ray experiment. This was achieved by visually comparing the observed and calculated patterns, using a fixed scale factor for the latter, and progressively adjusting the unit cell parameters on the assumption of approximately isotropic compression and minimal changes in the interaxial angles. Once sufficiently close agreement between observed and calculated peaks positions had been achieved, the subsequent powder pattern refinement proceeded smoothly and without difficulty, yielding structural parameters in excellent agreement with those obtained from the single-crystal X-ray study. The corresponding fit to the form I structure at 2.84 GPa (35 tonne load), just below the phase transition, is shown in Figure 2a.

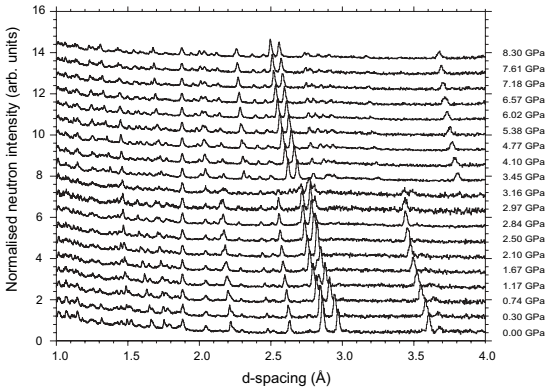

Figure 1. The sequence of neutron powder-diffraction data recorded, as a function of increasing pressure, through the form I and form III phase transition.

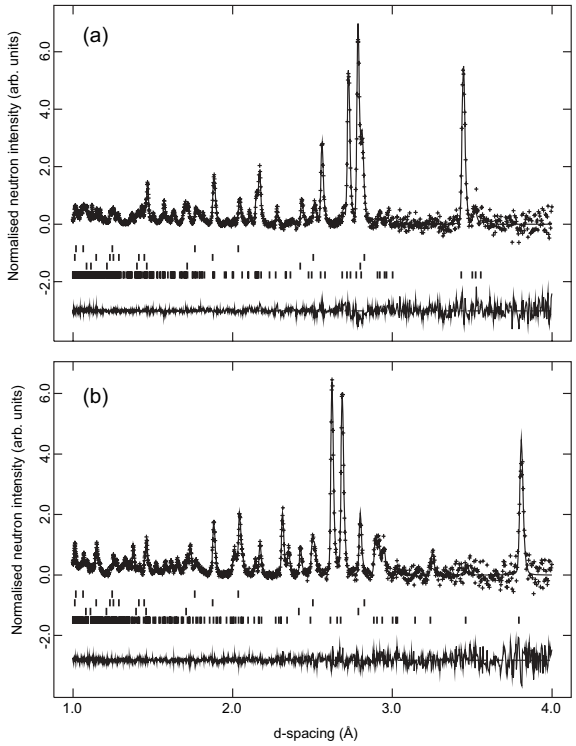

Figure 2. Rietveld profile refinements of the neutron powder-diffraction patterns of (**a**) the monoclinic, $P2_1/a$, form I (kalicinite) and (**b**) the triclinic, $P\bar{1}$, form III crystal structure of $KDCO_3$ at 2.84(5) and 3.45(5) GPa, respectively. In sequence from the bottom of the chart, the tick marks indicate reflections from the sample, the lead pressure marker and the weak reflections from the tungsten carbide nickel binder of the anvils.

Results and discussion

The unit-cell parameters and fractional coordinates obtained by Rietveld refinement of the neutron powder-diffraction data for

TABLE 2A. Crystallographic data for the monoclinic, $P2_1/a$, form I, obtained by high-pressure neutron powder-diffraction on pressure increase

Pressure (GPa)	0.00	0.30	0.74	1.17	1.67	2.10	2.50	2.84
a (Å)	15.195(3)	15.097(3)	14.945(2)	14.803(3)	14.663(2)	14.545(3)	14.419(2)	14.330(2)
b (Å)	5.6298(6)	5.6144(6)	5.588(5)	5.5641(6)	5.5384(6)	5.5216(6)	5.5011(5)	5.4868(4)
c (Å)	3.7088(4)	3.6932(4)	3.6691(5)	3.6509(5)	3.6323(5)	3.6211(5)	3.6093(5)	3.6024(4)
β (°)	104.534(10)	104.110(11)	103.538(10)	103.021(11)	102.527(10)	102.132(11)	101.731(10)	101.457(8)
V (Å^3)	307.11(5)	303.59(5)	297.90(5)	292.98(5)	287.96(5)	284.32(4)	280.31(4)	277.60(3)
K1								
x	0.1681(11)	0.1661(12)	0.1673(10)	0.1656(10)	0.1664(10)	0.1665(12)	0.1617(12)	0.1638(9)
y	0.030(4)	0.024(4)	0.021(4)	0.024(3)	0.027(3)	0.031(4)	0.033(3)	0.031(3)
z	0.302(5)	0.304(6)	0.300(5)	0.308(4)	0.309(4)	0.303(5)	0.298(4)	0.300(3)
C1								
x	0.1225(7)	0.1207(8)	0.1218(7)	0.1194(7)	0.1181(7)	0.1183(8)	0.1183(8)	0.1170(6)
y	0.520(3)	0.525(3)	0.530(3)	0.536(2)	0.534(2)	0.532(2)	0.536(2)	0.5357 (16)
z	0.860(3)	0.862(3)	0.870(3)	0.872(3)	0.865(3)	0.873(3)	0.878(3)	0.881(2)
D1								
x	0.0149(10)	0.0139(10)	0.0101(11)	0.0110(10)	0.0132(10)	0.0109(10)	0.0120(9)	0.0132(6)
y	0.694(2)	0.696(2)	0.694(2)	0.700(2)	0.701(2)	0.696(2)	0.699(2)	0.7010(17)
z	0.550(4)	0.546(5)	0.555(4)	0.548(4)	0.545(4)	0.552(4)	0.541(4)	0.543(3)
O1								
x	0.1945(8)	0.1960(8)	0.1953(8)	0.1952(8)	0.1941(9)	0.1926(9)	0.1954(7)	0.1940(6)
y	0.539(3)	0.537(3)	0.543(3)	0.540(3)	0.547(3)	0.549(3)	0.554(2)	0.5516(17)
z	0.100(4)	0.106(3)	0.111(3)	0.110(3)	0.113(3)	0.110(4)	0.118(3)	0.115(2)
O2								
x	0.0785(9)	0.0768(10)	0.0743(9)	0.0747(8)	0.0726(8)	0.0741(10)	0.0719(9)	0.0724(7)
y	0.722(2)	0.726(2)	0.718(2)	0.723(2)	0.725(3)	0.730(3)	0.737(2)	0.7360(17)
z	0.729(4)	0.728(4)	0.722(4)	0.725(4)	0.725(4)	0.736(4)	0.746(4)	0.740(3)
O3								
x	0.0835(10)	0.0850(11)	0.0842(10)	0.0841(9)	0.0855(10	0.0821(11)	0.0813(10)	0.0813(7)
y	0.323(2)	0.321(3)	0.323(3)	0.330(2)	0.328(2)	0.326(2)	0.327(2)	0.3287(15)
z	0.728(5)	0.728(5)	0.732(4)	0.726(4)	0.739(4)	0.750(4)	0.742(3)	0.750(2)
O2-D1	1.040(15)	1.035(16)	1.021(15)	1.024(16)	0.978(16)	1.033(17)	1.036(16)	1.011(12)
D1···O3	1.591(19)	1.590(21)	1.551(19)	1.540(19)	1.594(19)	1.554(19)	1.521(18)	1.550(13)
O2···O3	2.628(15)	2.621(17)	2.568(16)	2.564(15)	2.571(16)	2.582(17)	2.552(16)	2.558(12)
O2-D1···O3	174.6(1.6)	174.0(1.8)	173.8(1.9)	178.3(2.0)	177.3(1.8)	172.9(1.9)	172.5(1.7)	174.5(1.2)

TABLE 2B. Crystallographic data for the triclinic, $P\bar{1}$, form III crystal structure of deuterated potassium hydrogen carbonate, $KDCO_3$, obtained by high-pressure neutron powder-diffraction on pressure increase

Pressure (GPa)	3.45	4.10	4.77	5.38	6.02	6.57	7.18	7.61	8.30
a (Å)	6.3043(6)	6.2435(7)	6.1858(5)	6.1393(8)	6.0938(6)	6.0564(9)	6.0237(8)	5.9935(8)	5.9577(6)
b (Å)	5.3587(4)	5.3363(6)	5.3147(4)	5.2958(6)	5.2765(4)	5.2610(6)	5.2476(6)	5.2346(6)	5.2189(5)
c (Å)	4.2501(6)	4.2448(7)	4.2330(5)	4.2228(7)	4.2139(6)	4.2047(9)	4.1958(8)	4.1889(8)	4.1792(6)
α (°)	95.132(7)	95.216(9)	95.253(7)	95.297(10)	95.306(7)	95.293(10)	95.292(10)	95.298(11)	95.306(8)
β (°)	101.113(8)	100.935(9)	100.793(7)	100.665(9)	100.539(7)	100.438(11)	100.348(11)	100.273(11)	100.155(8)
γ (°)	109.326(7)	109.167(9)	109.016(6)	108.892(9)	108.786(7)	108.689(10)	108.578(10)	108.498(10)	108.412(7)
V (Å^3)	131.116(14)	129.357(18)	127.483(13)	125.933(17)	124.448(12)	123.175(19)	122.073(18)	121.061(19)	119.824(14)
K1									
x	0.302(2)	0.301(3)	0.3044(19)	0.300(2)	0.305(2)	0.299(3)	0.306(3)	0.301(3)	0.299(2)
y	0.1326(15)	0.130(3)	0.135(2)	0.130(3)	0.134(2)	0.129(3)	0.137(3)	0.132(3)	0.133(3)
z	0.293(3)	0.290(4)	0.300(3)	0.288(4)	0.296(3)	0.296(4)	0.295(4)	0.294(4)	0.289(3)
C1									
x	0.2329(14)	0.2317(16)	0.2316(11)	0.2272(16)	0.2322(12)	0.2309(18)	0.2317(18)	0.2332(18)	0.2315(14)
y	0.5738(15)	0.5735(18)	0.5740(13)	0.572(2)	0.5739(14)	0.573(2)	0.575(2)	0.570(2)	0.5733(17)
z	0.9117(17)	0.9133(19)	0.9098(15)	0.911(2)	0.9090(16)	0.908(2)	0.911(2)	0.909(2)	0.9120(18)
D1									
x	0.0836(15)	0.088(2)	0.0821(14)	0.0887(19)	0.0855(15)	0.084(2)	0.0849(19)	0.086(2)	0.0860(15)
y	0.7055(16)	0.703(2)	0.7063(14)	0.7071(18)	0.7056(14)	0.707(2)	0.705(2)	0.709(2)	0.7070(17)
z	0.541(2)	0.539(3)	0.537(2)	0.541(3)	0.539(2)	0.532(3)	0.538(3)	0.533(3)	0.533(2)
O1									
x	0.2084(15)	0.207(2)	0.2082(12)	0.2063(18)	0.2111(14)	0.2100(19)	0.208(2)	0.204(2)	0.2040(17)
y	0.7717(17)	0.774(2)	0.7732(15)	0.773(2)	0.7779(17)	0.775(2)	0.780(2)	0.774(3)	0.775(2)
z	0.7470(2)	0.750(3)	0.7452(19)	0.747(3)	0.748(2)	0.747(3)	0.742(3)	0.747(3)	0.749(3)
O2									
x	0.1110(14)	0.1102(18)	0.1094(13)	0.1097(19)	0.1110(15)	0.110(2)	0.111(2)	0.113(2)	0.1093(16)
y	0.3341(16)	0.3314(19)	0.3343(14)	0.333(2)	0.3325(16)	0.332(2)	0.330(2)	0.330(2)	0.3300(16)
z	0.771(2)	0.773(3)	0.7733(19)	0.776(3)	0.776(2)	0.776(3)	0.778(3)	0.768(3)	0.773(2)
O3									
x	0.3731(15)	0.3742(17)	0.3723(14)	0.3757(19)	0.3743(14)	0.376(2)	0.376(2)	0.376(2)	0.3738(17)
y	0.6425(18)	0.641(2)	0.6392(16)	0.643(2)	0.6403(17)	0.640(2)	0.638(3)	0.635(2)	0.6385(18)
z	1.179(2)	1.181(3)	1.179(2)	1.179(3)	1.179(2)	1.178(3)	1.176(3)	1.180(3)	1.175(2)
O1-D1	1.002(11)	0.999(15)	1.008(10)	0.973(14)	1.004(11)	1.023(17)	0.982(15)	0.992(16)	0.998(13)
D1···O2	1.568(13)	1.581(17)	1.541(11)	1.581(16)	1.565(13)	1.530(19)	1.562(18)	1.522(18)	1.520(14)
O1···O2	2.556(12)	2.555(15)	2.536(10)	2.537(15)	2.549(11)	2.537(16)	2.520(17)	2.496(17)	2.497(14)
O1-D1···O2	167.6(1.1)	163.9(1.5)	168.0(0.9)	166.3(1.2)	165.1(1.0)	167.1(1.5)	163.8(1.4)	166.0(1.6)	165.1(1.2)

forms I and III are presented in Tables 2a and 2b, respectively, along with selected bond lengths and bond angles. Views of the refined structures of form I, at 2.84 GPa, and form III, at 3.45 GPa, are shown in Figures 3a and 3b, respectively. The variation of the unit-cell parameters and unit-cell volume (expressed as volume per formula unit) with pressure are shown in Figures 4a and 4b, respectively. It is apparent that the phase transition is first-order in character, with a ~4% volume discontinuity at the transition. Third-order Birch-Murnaghan fits to the V(p) data both above and below the transition indicate that form III [B_0 = 26.5(2.8) GPa, B' = 5.2(6)] is marginally less compressible than form I [B_0 = 22.7(8) GPa, B' = 4.1(5)]. The form I equation of state parameters are in excellent agreement with those reported by Nagai et al. (2002).

As already stated, the form I crystal structure is characterized by the layers of $(HCO_3^-)_2$ dimers which are arranged on planes parallel to $(\bar{3}01)$ of the monoclinic unit cell. Neighboring layers are stacked such that slabs of dimers are formed which are separated by the K^+ cations. The principal features of the form I structure are largely preserved through the high-pressure phase transition and, as can be seen in Figure 3, the dimer layers would correspond closely to the $(\bar{2}01)$ plane of the triclinic unit cell. However, it is apparent that the dimers are tilted slightly with respect to these planes and they are, in fact, more closely parallel to the triclinic $(\bar{4}12)$ plane. The tilting appears to be in response to pronounced displacements of the K^+ cations at the transition so that more cation contacts are generated.

In both forms I and III, the K^+ cations are arranged in layers parallel to $(\bar{1}02)$ and $(\bar{1}01)$, respectively. For the form I structure, at 2.84 GPa there are eight $K^+\cdots K^+$ contacts that have distances ranging between 3.602(17) and 4.774(17) Å with an average contact distance of 4.221(18) Å (Fig. 5a). In the form III structure, at 3.45 GPa, the $K^+\cdots K^+$ contacts have a topology that is fairly similar to that of form I, although the range of distances is increased somewhat from 3.524(19) to 5.055(18) Å. Despite this apparent increase in the spread of the contact distances, the average $K^+\cdots K^+$ contact has marginally reduced in length to 4.192(18) Å after the phase transition.

As well as altering the $K^+\cdots K^+$ contacts at the phase transition, the displacements of the K^+ cations, accompanied by the cooperative tilting of the $(HCO_3^-)_2$ dimers, have a marked affect on the K···O coordination environment. In the form I structure, the K^+ cations are coordinated to eight oxygen atoms from six HCO_3^- anions, see Figure 6a, while in form III the coordination number increases to ten and a total of seven HCO_3^- molecules are involved in K···O contacts, as seen in Figure 6b. Apart from the increase in the coordination number at the transition, on the whole, the K···O distances themselves are largely preserved: i.e., at 2.84 GPa, the K···O distances range from 2.627(14) to 2.751(16) Å with an average distance of 2.751(16) Å; while at 3.45 GPa the K···O contacts range from 2.604(14) to 3.170(17) Å with an average distance of 2.844(14) Å.

As the O-D···O hydrogen bond distances in form I of $KDCO_3$ are relatively short, even at ambient pressure, they are considered to be moderately strong. In the study of the response of the form I structure to pressure by Kagi et al. (2003), it was found that the O···O distance shortened from 2.66–2.59 Å over the pressure interval 0–2.5 GPa, while the O-D···O angle decreased from 176–161°. In the current study, we find that the O···O distance exhibits a uniform and continuous compression

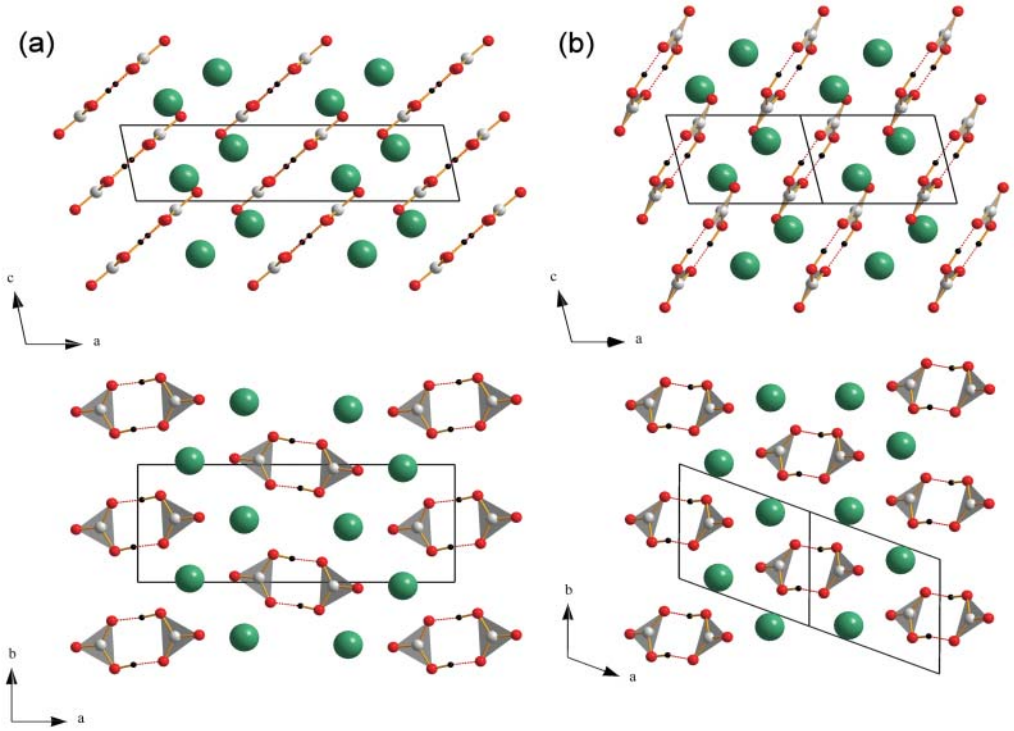

FIGURE 3. The crystal structures of (**a**) the monoclinic, $P2_1/a$, form I and (**b**) the triclinic, $P\bar{1}$, form III of potassium hydrogen carbonate, $KHCO_3$. In **b**, the structure is shown doubled along the crystallographic **a**-axis to aid comparison.

over the entire pressure range studied and, at least within error, the phase transition has little effect on the compressibility of the O···O distance (see Fig. 7c). Our results also indicate that the compressibility of the O···O distance over the form I region is in good agreement with that reported by Kagi et al. (2003)—although the distances reported in the current study are ~0.05 Å shorter on average. Both the O-D and D···O bond lengths show a smooth monotonic decrease over the pressure range studied (Figs. 7a and 7b, respectively) while for the O-D···O bond angle, there appears to be a discontinuity at the phase transition (Fig. 7d). After an initial, and very slight, reduction in the bond angle on compression

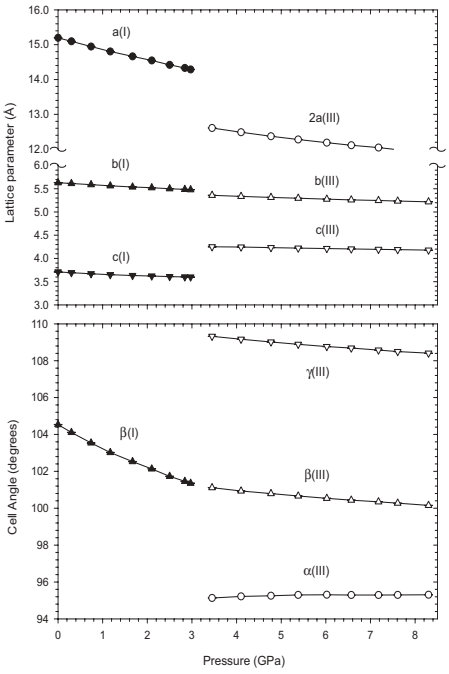

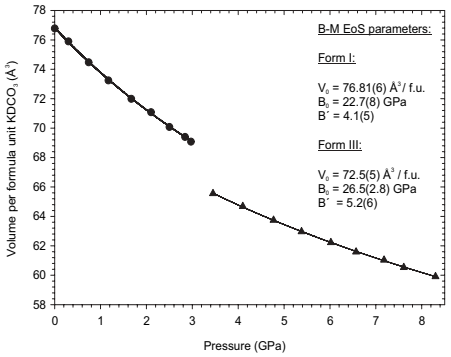

FIGURE 4. The variation of (**a**) the lattice parameters and (**b**) the unit-cell volume (expressed as volume per formula unit) with pressure for deuterated potassium hydrogen carbonate ($KDCO_3$).

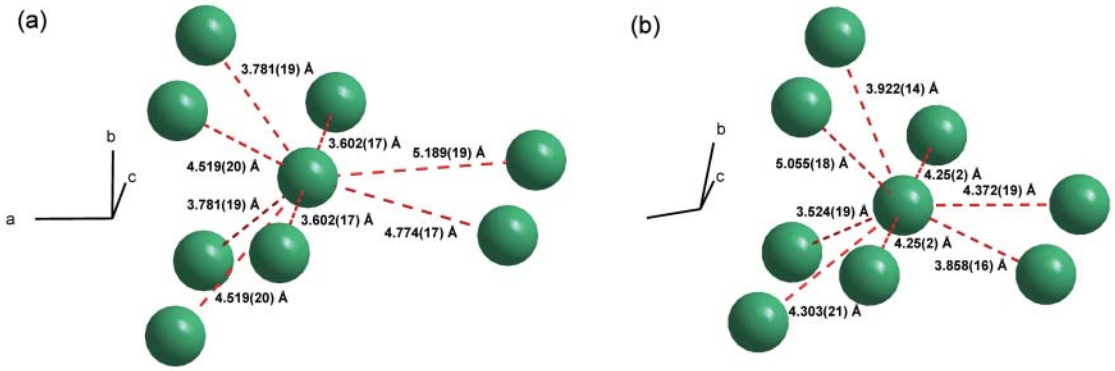

FIGURE 5. Projections of the K···K contacts in the (**a**) monoclinic, $P2_1/a$, form I and (**b**) the triclinic, $P\bar{1}$, form III crystal structures of $KDCO_3$. The $(DCO_3)_2$ dimers have been removed for clarity.

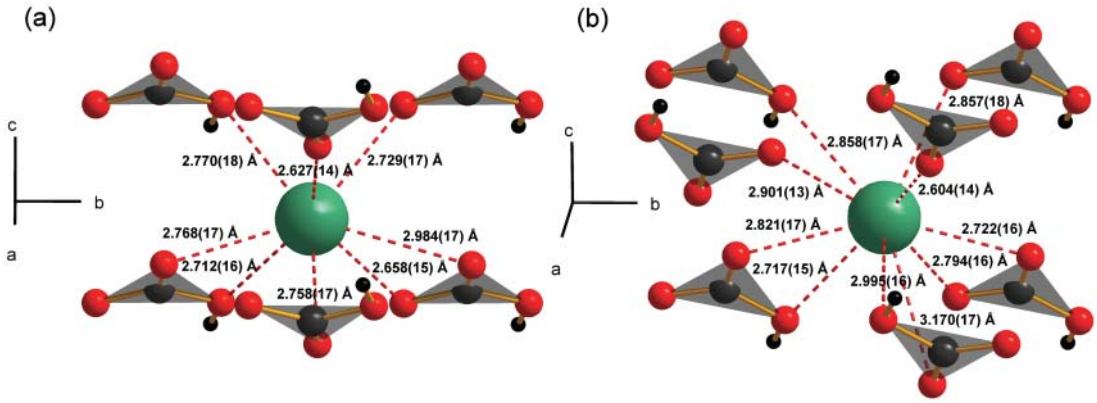

FIGURE 6. The potassium coordination environments in (**a**) the monoclinic, $P2_1/a$, form I and (**b**) the triclinic, $P\bar{1}$, form III crystal structures of $KDCO_3$.

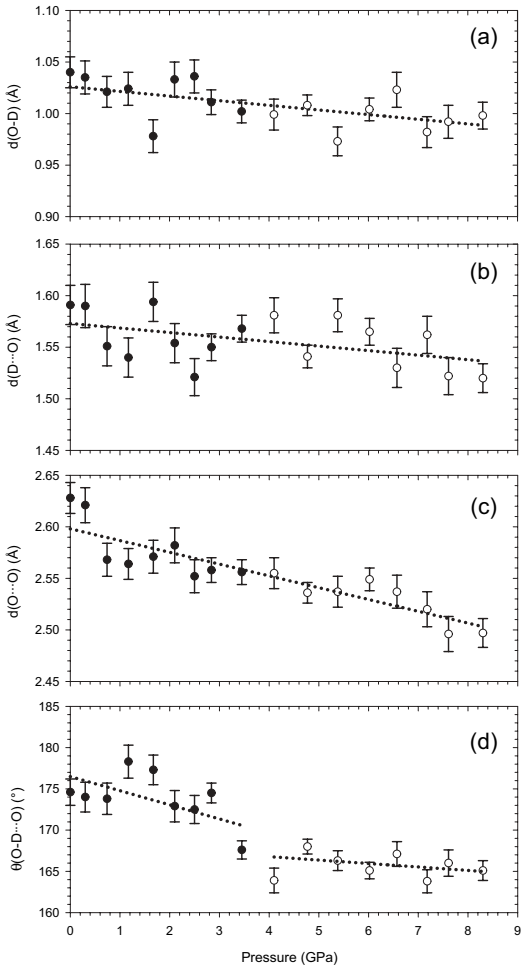

FIGURE 7. (**a**) The O-D (Å), (**b**) the D···O (Å), (**c**) the O···O (Å), and the O-D···O (°) hydrogen bond distances and angles in $KDCO_3$ as a function of pressure.

of the form I structure, there is an apparent ~4° angular decrease in the O-D···O bond during the transformation to the form III structure. Although the magnitude of this abrupt change is rather uncertain from the spread of the data, it is clear that there is a distinct change in the pressure dependence and, on subsequent compression, the O-D···O bond angle shows little further variation. The marked decrease in the O-D···O angle, and the change in its pressure dependence, suggests that the hydrogen bonding in the dimer becomes *weaker* at the transition. This is consistent with the sudden encroachment of the oxygen atom not involved in hydrogen bonding to form non-bonding inter-dimer O···O contacts, which have distances of 3.269(14) Å in the form I structure at 2.84 GPa and 2.919(13) Å in the form III crystal structure at 3.45 GPa.

There is also a marked difference between the topologies of the non-bonding O···O interactions for the form I and form III structures. In Figure 8, the four possible non-bonding O···O interaction topologies between $(HCO_3)_2$ dimers are depicted schematically. In type-I only the O atoms already forming the intra-dimer hydrogen bonds contribute to the interaction and a ladder-like chain is formed, as shown in Figure 8a. This arrangement is characteristic of the $KHCO_3$ form I crystal structure. The form III non-bonding O···O topology involves one of the O atoms forming the inter-dimer hydrogen bonds and the non-participating oxygen, O1, to form linear chains of type-II interactions, Figure 8b. The topology depicted in Figure 8d is composed of type-II interactions where the orientation of every alternate dimer is reversed so that zigzag chains are formed, and in Figure 8c the chains produced by linking alternate type-I and type-II interactions is illustrated. The latter is characteristic of the ambient form I crystal structure of another of the group-I carbonates, $CsHCO_3$ (Kaduk 1993).

The alteration of the topology of the non-bonding O···O interactions, has a profound effect on the proton ordering in the dimers. In the monoclinic form I structure, the $P2_1/a$ symmetry operations result in a reversal of the hydrogen atom positions in alternate layers of dimers arranged parallel to (002), as can

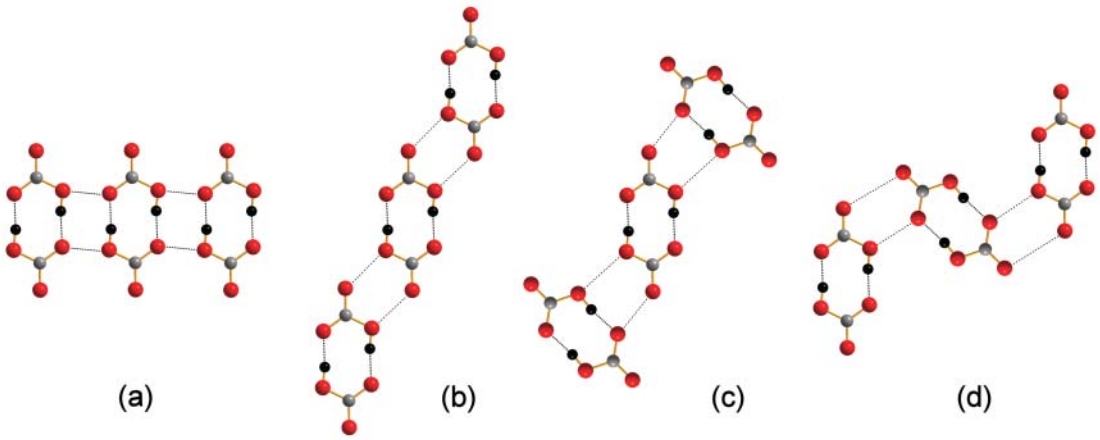

FIGURE 8. Possible non-bonding O···O interactions between neighboring $(HCO_3)_2$ dimers: (**a**) Type-I, characteristic of form I of $KHCO_3$; (**b**) and (**d**) Type-II, the former being characteristic of the high-pressure form III of $KHCO_3$; (**c**) alternating Type-I and Type-II interactions, characteristic of form I of $CsHCO_3$ (Kaduk 1993).

be seen in Figure 3a. In effect, the "orientation" of the dimers, with respect to the position of the hydrogen atoms, switches in an alternating sequence along the **a**-axis. In the form III structure this cell edge is effectively halved and there is an accompanying proton-transfer within the hydrogen bonds of dimers situated on consecutive layers. The overall changes in the hydrogen bonding remain fairly subtle, however, as the alteration in the hydrogen bonds are contained within the dimers, with no fundamental modification in the bonding topology. Similar proton-hopping behavior has been observed in several examples of both organic and inorganic materials (see for example Katrusiak et al. 1996 and Herbstein 2006).

ACKNOWLEDGMENTS

We are grateful to F.P.A. Fabbiani and S. Parsons for their help in the collection and processing of the high-pressure single-crystal data. We also thank the ISIS Facility of the CCLRC Rutherford Appleton Laboratory for the provision of neutron beam time and to D.J. Francis for his technical assistance during the neutron powder-diffraction experiments. We also thank the EPSRC for funding both this project and D.R.A.'s Advanced Research Fellowship.

REFERENCES CITED

Altomare, A., Gascarano, C., Giacovazzo, C., Gualardi, A., Burla, M.C., Polidori, G., and Camalli, M. (1994) SIR92—a program for automatic solution of crystal structures by direct methods. Journal of Applied Crystallography, 27, 435.

Besson, J.M., Nelmes, R.J., Hamel, G., Loveday, J.S., Weill, G., and Hull, S. (1992) Neutron powder diffraction above 10 GPa. Physica B**,** 180, 907–910.

Betteridge, P.W., Carruthers, J.R., Cooper, R.I., Prout, K., and Watkin, D.J. (2003) CRYSTALS, Version 12: Software for guided crystal structure analysis. Journal of Applied Crystallography, 36, 1487.

Bruker-AXS (2003) SAINT, Version 7. Bruker-AXS, Madison, Wisconsin.

Dawson, A., Allan, D.R., Parsons, S., and Ruf, M. (2004) The use of CCD detectors in crystal structure determinations at high pressure. Journal of Applied Crystallography, 37, 410–416.

Fillaux, F. and Cousson, A. (2004) Comment on "Quantum correlations between protons in potassium bicarbonate." Journal of Physics: Condensed Matter, 16, 1007–1010.

Fillaux, F., Cousson, A., and Keen, D. (2003) Observation of the dynamical structure arising from spatially extended quantum entanglement and long-lived quantum interference in the $KHCO_3$ crystal. Physical Review B, 67, 054301.

Forman, R.A., Piermarini, G.J., Barnett, J.D., and Block, S. (1972) Pressure measurement made by the utilization of ruby sharp-line luminescence. Science, 176, 284–285

Fortes, A.D. (2004) Computational and Experimental Studies of Solids in the Ammonia-Water System. Ph.D. thesis, University College, University of London.

Herbstein, F.H. (2006) On the mechanism of some first-order enantiotropic solid-state phase transitions: from Simon through Ubbelohde to Mnyukh. Acta Crystallographica, 62, 341–383.

ISIS (1996) Dedicated facility for high pressure diffraction. In ISIS 96—ISIS Facility Annual Report 1995–96, Rutherford Appleton Laboratory: 1996; Vol. RAL-TR-96-050, p. 61–62.

——— (1997) PEARL—Pressure and engineering research line. In ISIS 97—ISIS Facility Annual Report 1996–97, Rutherford Appleton Laboratory: 1997; Vol. RAL-TR-97-050, p. 28–29.

Kaduk, J.A. (1993) Crystal structure of caesium hydrogen carbonate, Zeitschrift fuer Kristallographie 205, 319–320.

Kagi, H., Nagai, T., Loveday, J.S., Wada, C., and Parise, J.B. (2003) Pressure-induced phase transformation of kalicinite ($KHCO_3$) at 2.8 GPa and local structural changes around the hydrogen atoms. American Mineralogist, 88, 1446–1451.

Kagi, H., Nagai, T., Komatsu K., Okada, T., Wada, C., Loveday, J.S., and Parise, J.B. (2005) Pressure response on hydrogen bonds in potassium hydrogen carbonate and sodium hydrogen carbonate. Journal of Neutron Research, 13, 21–26.

Kashida, S. and Yamamoto, K. (1990) Structural phase transition of $KHCO_3$. Journal of Solid State Chemistry, 86, 180–187.

Katrusiak, A. (1996) Stereochemistry and transformations of –OH–O= hydrogen bonds. Part II. Evolution of Tc in hydrogen-bonded ferroelectrics from structural data. Journal of Molecular Structure, 374, 177–189.

Keen, D.A. and Lovesey, S.W. (2003) Quantum correlations between protons in potassium bicarbonate. Journal of Physics: Condensed Matter, 15, 4937–4946.

Komatsu, K., Kagi, H., Nagai, T., Kuribayashi, T., Parise, J.B., and Kudoh., Y. (2005) Single crystal X-ray structure analysis of high pressure phase of Kalicinite, abstract k038-008, Earth and Planetary Science Joint Meeting, Japan.

Kuznetsov, A.Z., Dmitriev, V., Dubrovinsky, L., Prakapenka, V., and Weber, H.-P. (2002) FCC–HCP phase boundary in lead. Solid State Communications, 122, 125–127.

Larson, A.C. and Von Dreele, R.B. (2000) General Structure Analysis System (GSAS). Los Alamos National Laboratory Report LAUR 86–748.

Marshall, W.G. and Francis, D.J. (2002) Attainment of near-hydrostatic compression conditions using the Paris-Edinburgh cell. Journal of Applied Crystallography, 35, 122–125.

Merrill, L. and Bassett, W.A. (1974) Miniature diamond-anvil pressure cell for single-crystal X-ray diffraction studies. Review of Scientific Instruments, 45, 290–294.

Miller, R.A. and Schuele, D.E. (1969) The pressure derivatives of the elastic constants of lead. Journal of Physics and Chemistry of Solids, 30, 589–600.

Nagai, T., Kagi, H., and Yamanaka, T. (2002) The first observation of pressure-induced phase transition and compression behaviour of kalicinite ($KHCO_3$) at room temperature. Solid State Communications, 123, 371–374.

Nelmes, R.J., Loveday, J.S., Wilson, R.M., Besson, J.M., Klotz, S., Hamel, G., and Hull, S. (1994) Structure Studies at High Pressure Using Neutron Powder Diffraction. In J.D. Jorgensen and A.J. Schultz, Eds., Proceedings of the Symposium on Time-of-Flight Diffraction at Pulsed Neutron Sources, 29, p. 19–27. American Crystallographic Association, Buffalo, New York.

Nitta, I., Tomiie, Y., and Koo, C.H. (1952) The crystal structure of potassium bicarbonate, $KHCO_3$. Acta Crystallographica, 5, 292.

Parsons, S. (2004) SHADE. The University of Edinburgh, Scotland.

Sheldrick, G.M. (2004) SADABS. Bruker-AXS, Madison, Wisconsin.

Takasaka, S., Tsujimi, Y., and Yagi, T. (1997) Acoustic anomaly in the antiferrodistortive phase transition of $KHCO_3$ studied by Brillouin scattering. Physical Review B, 56, 10715–10718.

——— (2002) Shear-stress-induced transition in $KHCO_3$ studied by Brillouin scattering. Physical Review B, 65, 174102.

Thomas, J.O., Tellgren, R., and Olovsson, I. (1974) Hydrogen-bond studies. LXXXIV. An X-ray diffraction study of the structures of $KHCO_3$ and $KDCO_3$ at 298, 219 and 95 K. Acta Crystallographica B, 30, 1155–1166.

Waldorf, D.L. and Alers, G.A. (1962) Low-temperature elastic moduli of lead. Journal of Applied Physics, 33, 3266–3269.

MANUSCRIPT RECEIVED JUNE 1, 2006
MANUSCRIPT ACCEPTED JANUARY 24, 2007
MANUSCRIPT HANDLED BY PRZEMYSLAW DERA